STEM CELLS AND DEVELOPMENT
Volume 21, Number 5, 2012

DOI: 10.1089/scd.2011.0419

Isolation of Novel Multipotent Neural Crest-Derived Stem Cells from Adult Human Inferior Turbinate

Stefan Hauser,[1] Darius Widera,[2] Firas Qunneis,[1] Janine Müller,[1] Christin Zander,[2] Johannes Greiner,[1] Christina Strauss,[1] Patrick Lüningschrör,[2] Peter Heimann,[2] Hartmut Schwarze,[3] Jörg Ebmeyer,[3] Holger Sudhoff,[3] Marcos J. Araúzo-Bravo,[4] Boris Greber,[4] Holm Zaehres,[4] Hans Schöler,[4] Christian Kaltschmidt,[2] and Barbara Kaltschmidt[1]

Adult human neural crest-derived stem cells (NCSCs) are of extraordinary high plasticity and promising candidates for the use in regenerative medicine. Here we describe for the first time a novel neural crest-derived stem cell population within the respiratory epithelium of human adult inferior turbinate. In contrast to superior and middle turbinates, high amounts of source material could be isolated from human inferior turbinates. Using minimally-invasive surgery methods isolation is efficient even in older patients. Within their endogenous niche, inferior turbinate stem cells (ITSCs) expressed high levels of nestin, $p75^{NTR}$, and S100. Immunoelectron microscopy using anti-p75 antibodies displayed that ITSCs are of glial origin and closely related to nonmyelinating Schwann cells. Cultivated ITSCs were positive for nestin and S100 and the neural crest markers Slug and SOX10. Whole genome microarray analysis showed pronounced differences to human ES cells in respect to pluripotency markers OCT4, SOX2, LIN28, and NANOG, whereas expression of WDR5, KLF4, and c-MYC was nearly similar. ITSCs were able to differentiate into cells with neuro-ectodermal and mesodermal phenotype. Additionally ITSCs are able to survive and perform neural crest typical chain migration in vivo when transplanted into chicken embryos. However ITSCs do not form teratomas in severe combined immunodeficient mice. Finally, we developed a separation strategy based on magnetic cell sorting of $p75^{NTR}$ positive ITSCs that formed larger neurospheres and proliferated faster than $p75^{NTR}$ negative ITSCs. Taken together our study describes a novel, readily accessible source of multipotent human NCSCs for potential cell-replacement therapy.

Introduction

The neural crest was first described in 1868 by Wilhelm His as an intermediate chord ("Zwischenstrang") between the neural chord and the future ectoderm in the developing chick embryo [1]. During development, neural crest cells migrate out of the neural chord and give rise to several cell types of the mammalian organism like neurons, glial cells, or melanocytes [2]. In the head region of vertebrates neural crest cells differentiate into cells of both ectodermal and mesodermal fate [2].

Importantly, such neural crest-derived stem cells (NCSCs) can also be found in various adult tissues. They show extraordinary plasticity that can only be surpassed by embryonic stem cells (see [3] for discussion). In vitro NCSCs behave as multipotent self-renewing stem cells/progenitors [4] showing the ability to differentiate into multiple lineages [5,6]. Further, lineage tracing with either quail-chicken chimera [7,8] or with genetically tagged neural crest cells by Wnt1, Sox10, tPA, protein P0 promoter driven Cre recombinase showed multipotency of NCSCs in vivo (see [9] for review).

NCSCs from the head region were described in a number of adult organs and tissues like skin, cornea, hair follicles, periodontal ligament, palate, or pulpa of teeth [10–16]. It has been suggested that another NCSC-population is present within the olfactory epithelium. Genetic lineage tracing with Wnt1CRE crossed with R26RYFP showed that mouse neural crest cells directly formed so called olfactory ensheathing cells (OECs), glial cells that ensheathe the olfactory nerve [17]. Such neural crest related OECs can be found within embryonic [18] and adult olfactory mucosa [19]. Importantly, in humans, the olfactory mucosa is exclusively present in the middle and superior turbinate close to the cribriform plate (scheme, Fig. 1A) [see (20) for review].

[1]Molecular Neurobiology, University of Bielefeld, Bielefeld, Germany.
[2]Cell Biology, University of Bielefeld, Bielefeld, Germany.
[3]Klinik für Hals-, Nasen- und Ohrenheilkunde, Kopf- und Halschirurgie, Bielefeld, Germany.
[4]Department Cell and Developmental Biology, Max-Planck-Institute for Molecular Medicine, Münster, Germany.

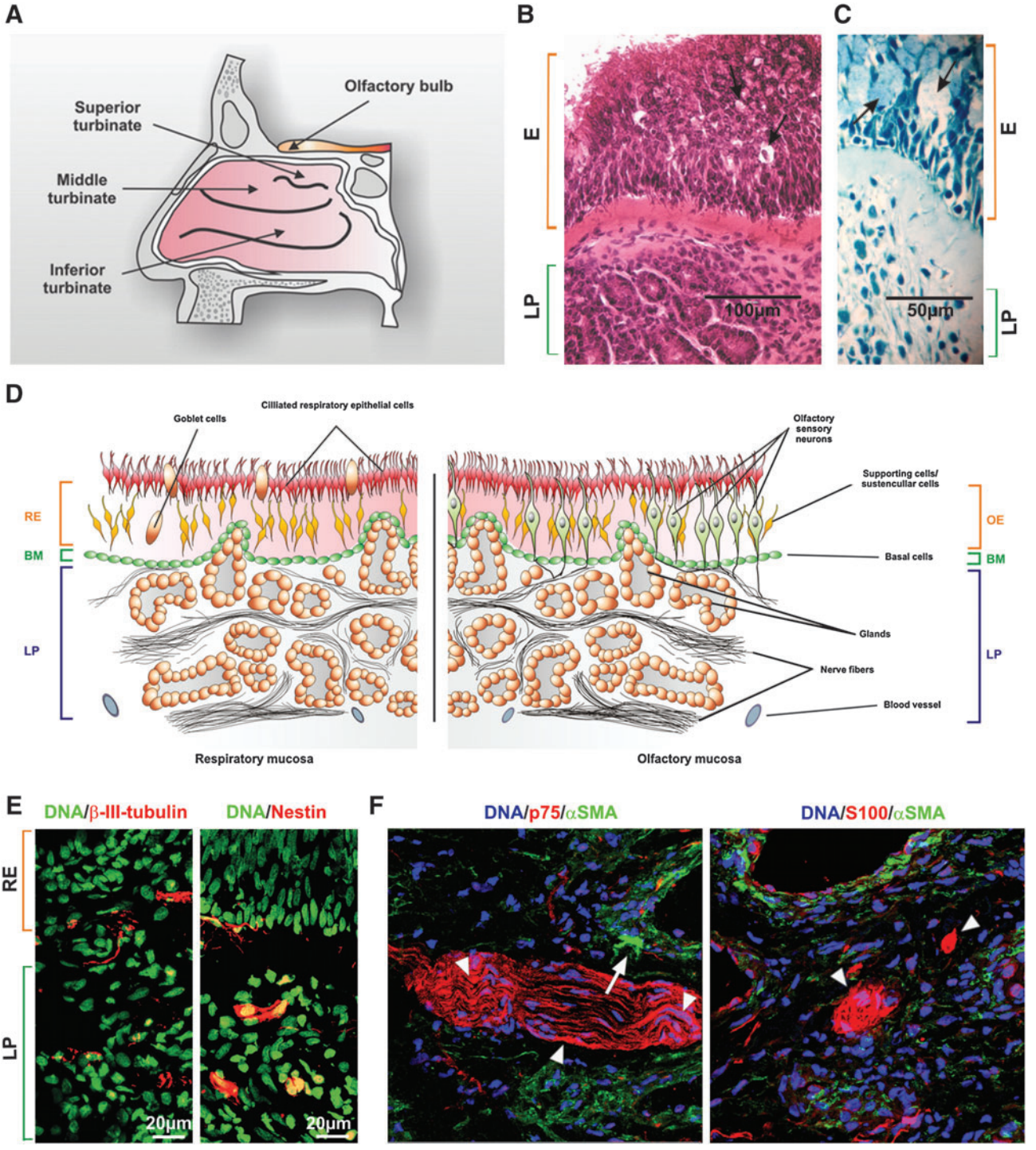

FIG. 1. Human inferior turbinates exclusively consist of respiratory mucosa without patches of olfactory mucosa **(A)** To localize ITSCs, human turbinates were obtained from the inferior turbinate of the nasal cavity. **(B)** HE staining of human turbinate showing the wide epithelial layer with ciliated surface. E: epithelium, LP: lamina propria. Scale bar: 100µm. **(C)** Richardson blue staining of human turbinate indicating goblets cells (*arrows*) within the epithelium. Scale bar: 50µm. **(D)** Schematic illustration of the morphological difference between respiratory and olfactory epithelium. RE: respiratory epithelium. OE: olfactory epithelium. BM: basement membrane. **(E)** Saggital sections of the human inferior turbinate. Sections were immunostained against nestin and β-III-tubulin, demonstrating that putative stem cells can be found within the LP. Binding of primary antibodies was visualised by appropriate secondary flurorochrome-coupled antibodies (*red*). Nuclei were stained with SYTOX Green. Scale bar: 20µm. **(F)** Double staining against p75/αSMA and S100/αSMA showed no co-expression of p75 (*red*) or S100 (*red*) with αSMA (*green*). Nuclei were stained with DAPI. *Arrows* demonstrating expression of p75 or S100 independent of αSMA. ITSCs, inferior turbinate stem cells; HE, hematoxylin-eosin; αSMA, smooth muscle actin.

We hypothesized that the respiratory mucosa of adult human inferior turbinate may contain at least 1 NCSC-population. In this study we identified for the first time neural crest-related stem cells within the respiratory epithelium of human adult inferior turbinate. We characterized the endogenous niche of these inferior turbinate stem cells (ITSCs) and describe their efficient isolation and cultivation. Further the expression pattern and differentiation potential of ITSCs has been investigated.

Material and Methods

Histochemical staining

Biopsied tissue of the human turbinate was used for cryostat sections. Frozen 10 μm thick sections were prepared on slides and subjected to hematoxylin-eosin (HE) staining as described in [16]. For Richardson blue (1% w/v methylene blue, 1% w/v Azur II) staining 2 μm semi-thin sections were stained for 60 s at 80°C and mounted with Entellan (Merck). The sections were examined using a bright field microscope (EVOS, Peqlab).

Immunohisto- and cytochemistry

Sections from turbinate sections were fixed in phosphate buffered 4% paraformaldehyde for 20 min at RT followed by 3 wash steps in 1xPBS. For immunocytochemistry, cultivated secondary neurospheres was seeded for 30 min on poly-D-Lysin coated Lab-Tek II chambers and fixed. The sections/cells were permeabilized with 0.02% Triton X-100 followed by incubation with primary antibodies for 2h at RT at the following dilutions: mouse anti-β-III-tubulin 1:100 (Promega), mouse anti-nestin 1:100 (Millipore), goat anti-p75 1:50 (Santa Cruz Biotechnology), mouse anti-p75 1:100 (Sigma-Aldrich), mouse anti-smooth muscle actin(αSMA) 1:50 (Sigma-Aldrich), rabbit anti-S100 1:100 (Dako), rabbit anti-β-III-tubulin 1:100 (New England Biolabs GmbH), mouse anti-vimentin 1:100 (Developmental Studies Hybridoma Bank), rabbit anti-NF-H 1:100 (Sigma-Aldrich), mouse anti-human nuclei 1:20 (Millipore), mouse anti-cytokeratin 14 1:100 (Millipore), and mouse anti-GFAP 1:100 (BD Biosciences). The secondary fluorochrome-conjugated antibodies were diluted 1:300 (Alexa 555 and Alexa 488, 1 h at RT). Nuclear counterstaining was performed with SYTOX green (1:20,000, Molecular Probes), TOTO (Invitrogen) or DAPI. Fluorescence imaging was performed using confocal microscopy (LSM 510, Carl Zeiss, and DM IRB, Leica) or fluorescence microscopy (AxioVert, Carl Zeiss).

Immunotransmission electron microscopy

Turbinate biopsies were dissected and fixed with perjodate-lysine-paraformaldehyde [21] for 3 h at 4°C. Fixed sections were infiltrated in phosphate buffered 30% saccharose overnight and cut into 45 μm thick sections at −22°C. Sections were blocked with 2% BSA and incubated free-floating in anti-p75 monoclonal antibody (1:100; Sigma) overnight at 4°C, incubated in anti-mouse-biotin antibody (1.5 h) and avidin-0.8 nm-nanogold (overnight; 4°C). Sections were postfixed in buffered 4% glutaraldehyde (30 min), washed in aqua dest, and nanogold was silver intensified by the Danscher-method [22]. Sections were postfixed in buffered 0.5% osmium tetroxide (15 min, 4°C) and flat-embedded in Araldite after dehydration and infiltration in an ascending series propylenoxide/resin at 50°C. Selected and documented areas were cut out, glued to a resin block, and sectioned into semi- and ultrathin sections. For electron microscopy 60–80 nm thick sections (stained for 40 min in uranyl acetate and 7 min in lead citrate) were inspected with a Zeiss EM 109.

Reverse transcription PCR

Total RNA was isolated using the RNeasy Mini Kit (Qiagen) with on-column DNA digestion according to the manufacture's guidelines. RNA yield and quality were assessed via Nanodrop UV spectrophotometry. cDNAs were generated via reverse transcription of 1.0 μg total RNA using the First Strand cDNA Synthesis Kit (Fermentas). PCR was performed using the KAPA2G Robust PCR Kit (Peqlab) according to the manufacturer's guidelines and 0.5 μM primers (Metabion). The cycling conditions comprised an initial denaturation of 1 min at 94°C and 35–38 cycles of 15 s at 94°C, 15 s at the appropriate temperature, and 20 s at 72°C followed by a final elongation for 1 min at 72°C. For primer sequences see Supplementary Table S1.

Western blot

Tissue samples were lysed on ice using 500 μL of lysis buffer (10 mM Tris, 1%SDS, 3 mM EDTA) and homogenized in a rotor-stator. Lysates were centrifuged for 10 min at 10000 rpm (4°C) and 16 μL of the supernatant was mixed with 4 μL 5× loading buffer and heated for 5 min at 94°C, subjected to electrophoresis on 12% denaturing SDS polyacrylamide gels, and transferred with a semi-dry blotter to a nitrocellulose membrane (Carl Roth GmbH). Blots were blocked and incubated with the first antibody after incubation with a HRP-linked secondary antibody. The results of the blot were visualized using enhanced chemiluminescence.

Cell isolation and culture of ITSCs

Turbinates were obtained by biopsy during routine nasal surgery, after an informed consent according to local and international guidelines (Bezirksregierung Detmold/Münster).

Biopsy tissues were immediately placed in PBS on ice followed by mechanical mincing using the Mcllwain Tissue Chopper. Afterward, the tissue was dissociated using Collagenase I (Sigma-Aldrich; 0.3 units/mL, 90 min, 37°C) followed by mechanical trituration. The primary cultures were grown for at least 72h in serum-free medium consisting of Dulbecco's modified Eagle's medium/Ham F-12 (DMEM/F-12; Invitrogen) supplemented with basic fibroblast growth factor-2 (FGF-2; 40 ng/mL), epidermal growth factor (EGF; 20 ng/mL; R&D Systems), Heparin (2 μg/mL, Sigma-Aldrich), and B27 supplement. For rapid expansion, ITSCs were cultivated using DMEM/F-12 supplemented with 10% human blood plasma, 40 ng/mL FGF-2, and 20 ng/mL EGF.

Scanning electron microscopy

Neurospheres were briefly washed with phosphate buffer, fixed in 4% glutaraldehyde and 2% paraformaldehyde in phosphate buffer for 2 h. After washing 4 times for 2 min at

RT cells were postfixed in the dark in 2% osmiumtetroxide, 1.5% potassium hexacyanoferrate in 100 mM phosphate buffer, pH 7.2. Dehydration of samples was done in an ascending acetone series and subsequent critical point-drying. Sputter-coated spheres were analyzed in a scanning electron microscope (Zeiss LEO1530).

Whole genome expression analysis

500 ng of total RNA per sample was used as input into a linear amplification protocol (Ambion) which involved synthesis of T7-linked double-stranded cDNA and 12 h of in vitro transcription incorporating biotin-labeled nucleotides. Purified and labeled cRNA was then hybridized for 18h onto HumanHT-12 v4 expression BeadChips (Illumina) following the manufacturer's instructions. After washing as recommended, chips were stained with streptavidin-Cy3 (GE Healthcare) and scanned using the iScan reader (Illumina) and accompanying software. Samples were exclusively hybridized as biological replicates.

Microarray data processing

The bead intensities were mapped to gene information using BeadStudio 3.2 (Illumina). Background correction was performed using the Affymetrix Robust Multi-array Analysis background correction model [23]. Variance stabilization was performed using the log2 scaling and gene expression normalization was calculated with the method implemented in the lumi package of R-Bioconductor. Data postprocessing and graphics was performed with in-house developed functions in Matlab.

The microarray data discussed in this publication have been deposited in NCBI's Gene Expression Omnibus [24] and are accessible through GEO Series accession number GSE30596.

(www.ncbi.nlm.nih.gov/geo/query/acc.cgi?token=vrojpyegcaqqkrq&acc=GSE30596).

Teratoma formation assay

ITSCs from 3 independent donors were subcutaneously injected into the dorsal flank of severe combined immunodeficient (SCID) mice ($1–2\times10^6$ cells/mice, $n=6$). The mice were observed for 20 weeks and no teratoma formation was detectable. As a positive control human iPS cells, which were injected in parallel, gave rise to teratomas within 6–8 weeks [25].

Real-time PCR

All qPCR reactions were performed as triplicate using Platinum SYBR Green qPCR Super-Mix UDG (Invitrogen) and assayed with a Rotor Gene 6000 (Qiagen).

Proliferation assay

Dissociated secondary neurospheres were cultivated in presence of growth factors in defined cultivation media containing 10% human blood plasma for a period of 4 days. The total cell numbers were measured each 24 h using the Cellometer Auto T4 (Peqlab). Cells were harvested by enzymatic dissociation and cell numbers were determined in triplicates. For analysis of population doubling time GraphPad Prism 5 was applied.

Limited dilution- and self-renewal assay

Long-term sphere formation was analyzed by measuring the diameter of growing secondary spheres over 3 passages. Diameter of ITSC-spheres was calculated by analyzing microscopic images with ImageJ software (NIH).

To analyze the clonogenic efficiency of ITSCs, a limited dilution assay was performed as described in [16]. Clones were analyzed over a time period of 2 months.

To identify the self-renewal capacity of ITSCs, tertiary ITSC clones were dissociated, plated at clonal density, and cultivated in DMEM containing 10% FCS for 14 days. To identify multi-lineage differentiation of single cell clones immunocytochemical stainings were performed as described.

Measurement of DNA content for cell-cycle analysis

For DNA content analysis CyStain PI absolute T-Kit was used (PARTEC) according to the manufacturer's guidelines. 1×10^6 cells per sample were harvested and lysed with 70% ethanol. The PI staining was analyzed on a CyFlow space instrument (PARTEC) and data gated for doublet exclusion using FL3-A versus FL3-W method with the FlowJo software (Tree Star).

Induced neuronal differentiation

For induced neuronal differentiation, dissociated secondary neurospheres were re-suspended in DMEM (Sigma-Aldrich) containing 10% FCS (Sigma-Aldrich) an plated at a density of 5×10^4 cells per 12 Well. After 48 h, 1 μM dexamethasone (Sigma-Aldrich), 2μM insulin (Sigma-Aldrich), 500μM 3-isobutyl-1-methylxanthine (Sigma-Aldrich), 200μM indomethacin (Sigma-Aldrich) and 200μM ethanol were added to the medium to induce neuronal differentiation. After 28 days, RNA isolation, immunocytochemical stainings and detection of synaptic vesicle recycling was performed as described below.

Vesicle recycling

Detection of vesicle recyling was analyzed in ITSCs differentiated for 28 days in neuronal induction medium using FM 1–43 Lipophilic Styryl Dyes (Life Technologies, Molecular Probes) according to the manufacturer's guidelines. Cells were washed in HBSS (Sigma-Aldrich), stimulated with 75 mM KCl and immediately stained for 90 s with FM 1–43 dye. Fluorescence imaging was performed using fluorescence microscopy (AxioVert, Carl Zeiss).

Spontaneous differentiation assay

Dissociated secondary neurospheres were resuspended in DMEM containing 10% FCS for mesodermal differentiation and plated at 1×10^5 cells per well in 24-well plates. After at least 7 days of differentiation, cells were fixed and processed for immunocytochemical analysis.

Adipogenic differentiation

For adipogenic differentiation, ITSCs were cultivated in DMEM (Sigma-Aldrich) containing 10% FCS (Sigma-Aldrich) and plated at a density of 4×10^3 cells per well in

12-well plates. After 48 h, 1 μM dexamethasone (Sigma-Aldrich), 2μM insulin (Sigma-Aldrich), 500μM 3-isobutyl-1-methylxanthine (Sigma-Aldrich), 200μM indomethacin (Sigma-Aldrich) was added to medium and cultivated for 72h. Afterwards the medium was switched and cells were cultivated in DMEM containing 10% FCS and 2μM insulin (Sigma-Aldrich) to induce adipogenic differentiation for 4 days. These two media were alternatingly used and changed every 4 days for 3 weeks. Subsequently cells were fixed in 10% PFA for 60 min and stained with Oil Red O (Sigma-Aldrich).

Chondrogenic differentiation

For chondrogenic differentiation, 2×10^6 ITSCs were cultivated in DMEM (Sigma-Aldrich) containing 10% FCS (Sigma-Aldrich), 10 ng/ml TGF-β1 (Peprotech GmbH, Hamburg, Germany) 0.1μM dexamethasone (Sigma-Aldrich) and 1% ITS-supplement as high density pellet culture for 28 days. Subsequently paraffin sections were made and stained with Alcian blue (Sigma-Aldrich) to detect the presence of glycosaminoglycans.

Osteogenic differentiation

For osteogenic differentiation, ITSCs were cultivated in DMEM (Sigma-Aldrich) containing 10% FCS (Sigma-Aldrich) at a densitiy of $3\times10^3/cm^2$ for 48h. Afterwards cells were cultivated for 18 days in presence of 100 nM dexamethasone (Sigma-Aldrich), 10 mM β-glycerophosphate (Sigma-Aldrich) and 0.05 mM L-ascorbic acid-2-phosphate (Sigma-Aldrich) to induce osteogenic differentiation. The ALP activity was measured in differentiated ITSCs using the Alkaline Phosphatase Detection Kit (Millipore) according to the manufacturer's guidelines. To detect biological mineralization, cells were fixed in 4% PFA for 15 min and stained with Von Kossa and Alizarin Red S (Waldeck GmbH).

Lentiviral transduction

Lentivirus production was perfomed by co-transfection of 293FT cells using calcium-phosphate precipitation. 1×10^7 cells were plated on a 15 cm dish and transfected with FUG-W transfer plasmid, Δ8.91, VSV-G helper plasmids and plasmid cFUG-W/pWPT-nlsLacZ. 60–72 h after transfection the supernatant was harvested and stored at −80°C or used immediately for concentration by ultracentrifugation (50.000g, 2 h, 4°C). High titer lentivirus and polybrene was added to 5×10^4 ITSCs (negative for HBV/HCV/HIV) or HEK293T and incubated for 24 h. Afterwards GFP-ITSCs/LacZ-ITSCs or LacZ-HEK293T were washed and used for injection. For the injection 2 different transgenes were used to exclude the influence of the GFP or LacZ transgenes on the experimental outcome.

In vivo transplantation

Fertile chicken eggs were incubated at 37°C until Hamburger-and-Hamilton stage 15–18. Small openings were made at the side of the shell and stained with 0.05% Fast Green (Roth). An incision was made to create a lesion into the third lastly formed somite. 5×10^3 GFP-ITSCs ($n=9$), LacZ-ITSCs ($n=5$) or LacZ-HEK293T ($n=4$) were injected into the lesion site and the embryos incubated for additional 72h. Afterward 5 embryos with injected ITSCs and 4 embryos with HEK293T were removed, quickly decapitated, eviscerated, fixed in 4% paraformaldehyde/PBS, and embedded in paraffin. Embryos were sectioned at 4.8 μm thickness, deparaffinized, and antigen unmasked for further staining method (see immunohistochemistry).

Magnetic sorting of $p75^{NTR+}$ ITSCs, magnetic cell sorting

Freshly dissociated inferior turbinate samples were passed through 30 μm filter (Celltrics, PARTEC) and divided into 2 fractions. The first fraction was labeled and separated using the CD271 MicroBead Kit (PE) (Miltenyi Biotec, Bergisch Gladbach, Germany) according to the manufacturer's instructions using LS separation columns. The second fraction, used as control, was labeled with PE-coupled IgG1.PE control antibody (Miltenyi Biotec). After separation, the isotype control-, the nonenriched-, negative-, and positive fractions were processed for flow cytometric analysis and subsequent experiments.

Flow cytometric analysis of ITSCs

A total number of 100.000 events were analyzed on a CyFlow space flow cytometer (PARTEC) directly after magnetic separation. Data acquisition was performed using the FlowMax software (PARTEC). Data were reanalyzed using FlowJo software (Tree Star, OR, USA).

Results

Human inferior turbinates exclusively consist of respiratory mucosa without patches of olfactory mucosa

To ensure that the tissue of the inferior turbinate (scheme in Fig. 1A) exclusively contains respiratory mucosa and no islet of olfactory mucosa, the morphology of this tissue was examined (Fig. 1B). The respiratory mucosa is easily distinguishable from the olfactory mucosa, since it is generally more expanded [26] and displays unique features. A typical morphology of multilayered respiratory epithelium with large ciliated surface was observable (Fig. 1B). Further, several goblet cells could be detected, which are a typical hallmark of respiratory mucosa (Fig. 1C, *arrows*).

The olfactory mucosa is subdivided into the olfactory epithelium (OE), containing the sensory neurons and the underlying lamina propria (LP) consisting of nerve fibers, connective tissue, glands, and blood vessels (Fig. 1D). A distinguishing mark of olfactory mucosa is the presence of β-III-tubulin- and neurofilament-positive olfactory sensory neurons in the epithelial layer [27,28]. Immunohistochemical staining against β-III-tubulin (Fig. 1E) and neurofilament (data not shown) revealed the absence of marker-positive sensory neurons in the epithelial layer, but several positive cells within the LP.

Putative stem cells are localized adjacent to nerve fibers within the lamina propria of respiratory mucosa

To investigate the endogenous niche of potential NCSCs within respiratory mucosa, tissue sections were stained

against nestin. Strong expression was observed close to the nerve fibers within LP (Fig. 1E). Weak nestin expression was detected in basal cells of the epithelium (Fig. 1E), which represent an epithelial stem cell population within nasal mucosa [29].

Then, sections were stained against the neural crest marker $p75^{NTR}$. Positive cells were observed within LP adjacent to the nerve fibers (Supplementary Fig. S1A). Further, S100, a marker for OECs and Schwann cells, was only detected within LP (Supplementary Fig. S1B).

Stem cells within LP of respiratory epithelium are nonepithelial cells

To prove a potential epithelial origin of ITSCs, sections were stained against cytokeratin 14 (CK14), a well established marker for epithelial layer of both olfactory and respiratory mucosa [30]. CK14 expression was detected in basal cells of the epithelial layer of respiratory mucosa, but not in cells adjacent to nerve fibers, which express nestin, p75, and S100 (Supplementary Fig. S2A). Interestingly, CK14 was also detected in glands within LP.

Respiratory lamina propria contains stem cells distinct from OECs

Since OECs could be present in LP even if β-III-tubulin positive signal was not detected in the epithelium, sections were stained with antibody specific for GFAP, which is found in OECs [31]. Marker-positive cells were detected exclusively within LP but not in the epithelial layer (Supplementary Fig. S2B).

It has been reported that OECs express αSMA in vivo and in vitro [32]. Double-staining of sections against p75/αSMA and S100/αSMA demonstrated that ITSCs were positive for both p75 and S100 while no αSMA co-expression was detected (Fig. 1F).

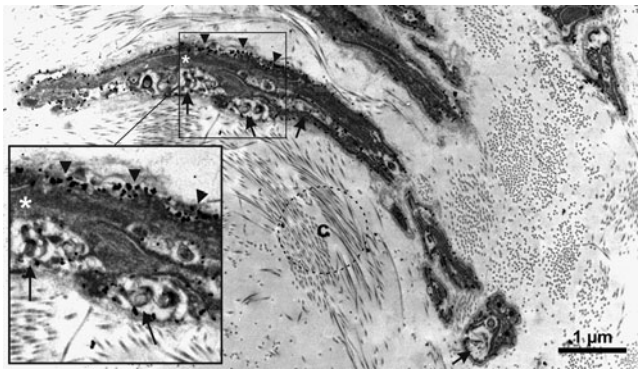

FIG. 2. p75 positive Schwann cell-like ITSCs were closely located to nerve fibers. Nerve fibers were embedded to connective tissue containing collagen fibers (c). p75 expression was detectable by nanogold silver-intensified particles which were identified at the surface of the cell membrane (*arrowheads*). *Arrows* indicate axons closely related to nonmyelinating Schwann cells (*asterisk*). Scale bar: 1µm.

ITSCs are of glial origin

By transmission electron microscopy using an anti-p75 antibody coupled to nanogold silver-intensified particles (arrowheads) ITSCs were identified closely located to nerve fibers (Fig. 2). Nanogold particles were attached to the cell surface membrane of cells with similar morphology and localization as nonmyelinating Schwann cells. This cell type can be found near to axons (arrows). Labeling with isotype control antibody revealed no specific signal (Supplementary Fig. S3).

Expression pattern of ITSCs in their niche

As further proof of the presence of a novel stem cell population within inferior turbinate tissue, PCR analysis of

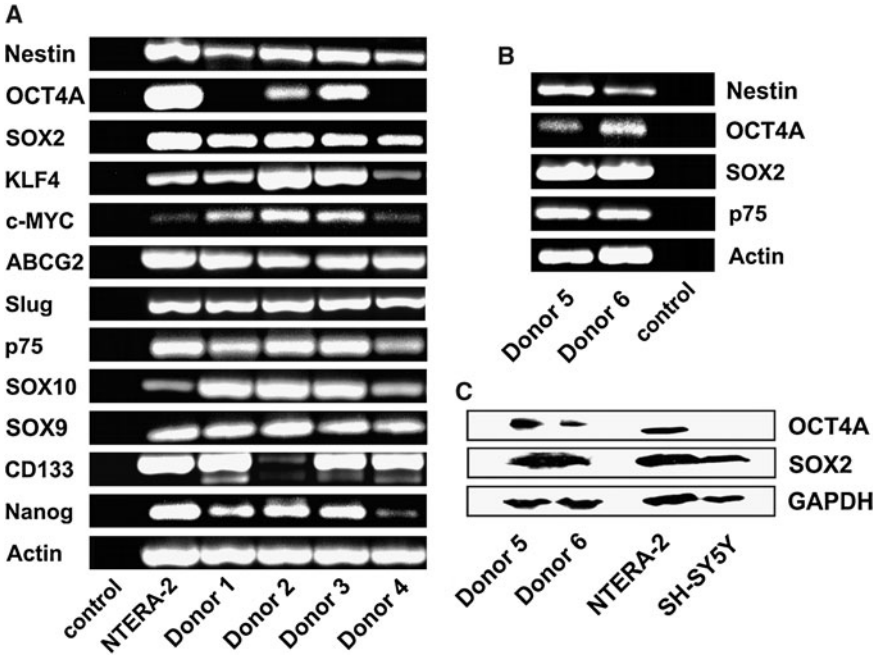

FIG. 3. Expression pattern of ITSCs in their niche. **(A)** Reverse transcriptase PCR analysis shows that cells within the tissue were related to neural crest (SOX9, SOX10, p75, and Slug), expressed the stemness marker nestin and ABCG2 and the so called "pluripotency factors" SOX2, KLF4, c-MYC, OCT4A, and NANOG. cDNA was normalized using the housekeeping gene β-Actin. NTERA-2 cells line was used as control template **(B)** Detection of the transcription factors SOX2 and OCT4 via western blot in 2 different donors. GAPDH was used as housekeeping gene and NTERA-2/SH-SY5Y as control cell lines. **(C)** PCR analysis of the same donors demonstrated the conformability of the western blot.

neural crest and stemness marker genes was performed (Fig. 3A). Tissue samples were positive for the neural crest markers SOX9, SOX10, p75, and Slug. Further, the stem cell markers nestin and ABCG2 were strongly expressed indicating the presence of putative stem cells in all examined tissues. This assumption is supported by the expression of the so called "pluripotency factors" - SOX2, KLF4, c-MYC, and NANOG. Interestingly OCT4A was only detectable in 2 of 4 analyzed tissues. However, the expression level of OCT4A, SOX2, and NANOG was obviously lower than in the NTERA-2 control.

To verify the results obtained by PCR, tissue samples were assayed using western blot to detect OCT4 and SOX2 at protein level. In case of OCT4 this detection is essential because different pseudogenes could be identified resulting in possible misinterpretation of data. The expected 34 kDa band

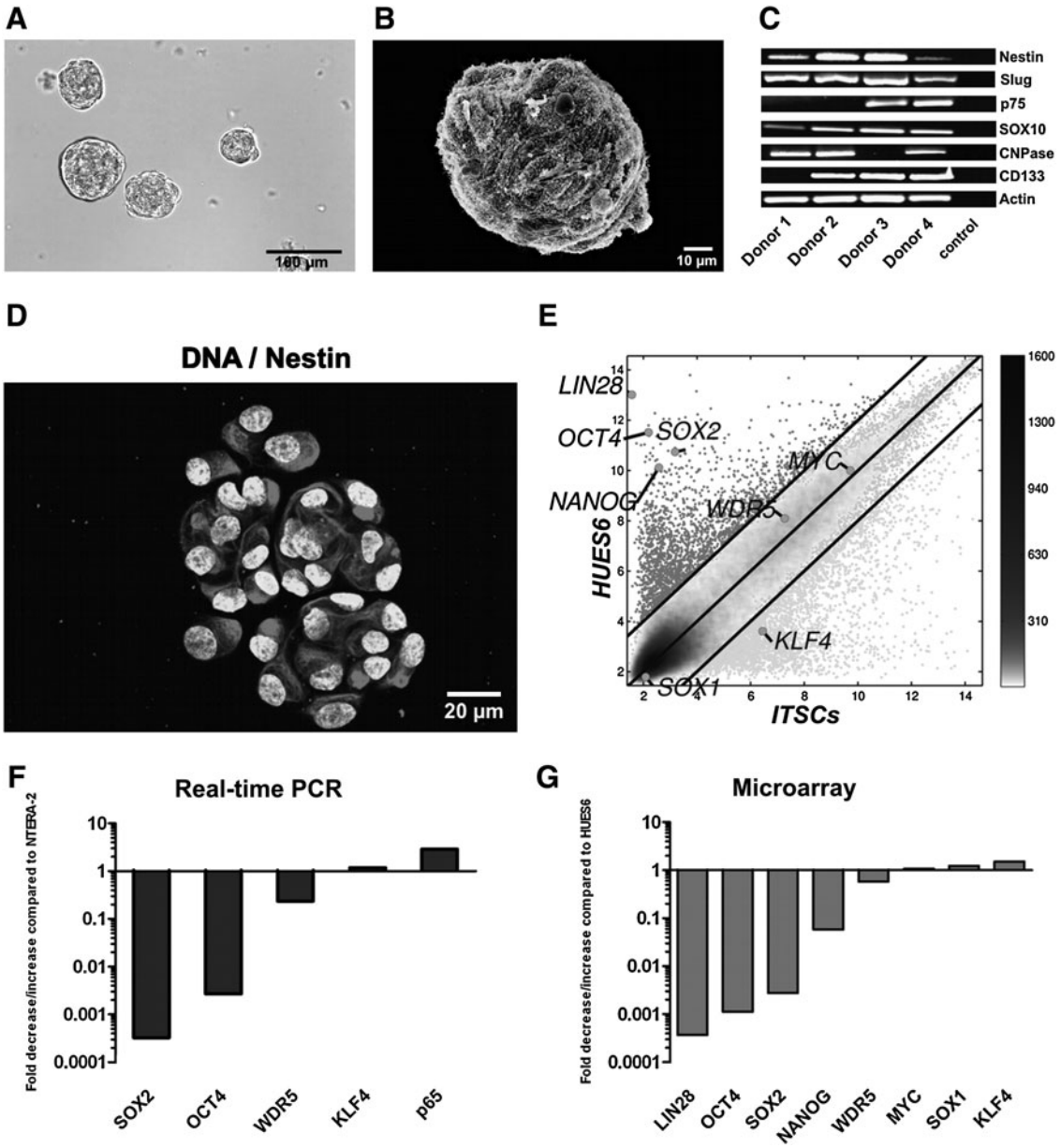

FIG. 4. Characterization of in vitro expanded ITSCs. **(A)** Secondary neurospheres formed from cells cultured from biopsy of human turbinates. Scale bar: 100 µm. **(B)** Scanning electron microscope image of a secondary neurosphere. Scale bar: 10 µm. **(C)** Reverse transcriptase PCR analysis showed the expression of the stem cell marker nestin, the neural crest-related transcripts Slug, p75, and SOX10 and the Schwann cell marker CNPase. cDNA was normalized using the housekeeping gene β-Actin. **(D)** Immunocytochemical staining showed that neurospheres are positive for the stemness marker nestin. Nuclei were stained with SYTOX *Green*. Scale bar: 20µm **(E)** Comparison of gene expression of the transcription factors and genes important for reprogramming. C-MYC, WDR5, and KLF4 are expressed by ITSCs at the same level or even higher, whereas OCT4, SOX2, LIN28, and NANOG are expressed at lower levels compared with HUES6. **(F)** Verification of the results from microarray experiments by real-time PCR. SOX2 and OCT4 are expressed at a lower level compared with NTERA-2 whereas WDR5 and KLF4 are nearly expressed at the same level. **(G)** Expression level of pluripotency-associated transcripts as measured by microarray analysis.

for SOX2 and the 52 kDa band for OCT4 were visualized (Fig. 3C). The expression of SOX2 and OCT4 within the same donors at RNA-level (Fig. 3B) was clearly confirmed at protein level (Fig. 3C).

Neurosphere forming stem cells can be isolated from inferior turbinate and cultivated in vitro

ITSCs cultivated under serum-free conditions in the presence of FGF-2 and EGF formed neurospheres after at least 4 days (Fig. 4A). While cells within the neurosphere are small and compact, superficial cells are flattened and longitudinally shaped and bear numerous microvilli as shown by scanning electron microscopy (Fig. 4B).

Cultivated ITSCs express neural crest and stemness markers

To characterize the population of ITSCs, the expression of neural crest and stemness markers was analyzed using PCR (Fig. 4C). All tested donors were positive for nestin. Further, all cultivated cells showed an expression of neural crest markers Slug and SOX10, whereas p75 was detectable in 2 of 4 tested cell cultures. Interestingly CNPase, a marker for Schwann cells or oligodendrocytes, was detectable in 3 of 4 analyzed donors.

For further characterization, the protein expression of nestin was assayed using immunocytochemistry. ITSCs showed high expression of nestin (Fig. 4D) and of S100 (Supplementary Fig. S4A).

Microarrays covering transcripts from the whole human genome were used to analyze the expression pattern of ITSCs. Microarray experiments showed that the expression of c-MYC, KLF4, and WDR5 is in the same range or even higher compared with the hESC-line HUES6 (Fig. 4E). Other important pluripotency factors (OCT4, LIN28, SOX2, and NANOG) are significantly lower expressed by the ITSCs. The results shown in Fig. 4E could be reproduced using 5 different patients with comparable results (Supplementary Fig. S5). These findings were verified by Real-time PCR. ITSCs expressed lower levels of OCT4 and SOX2 compared with human teratoma cell-line NTERA-2 (Fig. 4F). WDR5 and KLF4 are almost identically expressed, whereas the nuclear factor NF-κB subunit p65 is higher expressed in ITSCs.

ITSCs are highly proliferative and show normal DNA content

Proliferation of cultivated ITSCs was also analyzed by determining the total cell number every 24 h. ITSCs proliferated without morphological signs of differentiation and had a population doubling time of 33.1h (Fig. 5A).

Ploidy of ITSCs was investigated by flow cytometric analysis of PI-stained DNA. Cultivated ITSCs showed a typical DNA content for diploid cell cultures even after 90 days of cultivation (Fig. 5B). The long-term genetic stability

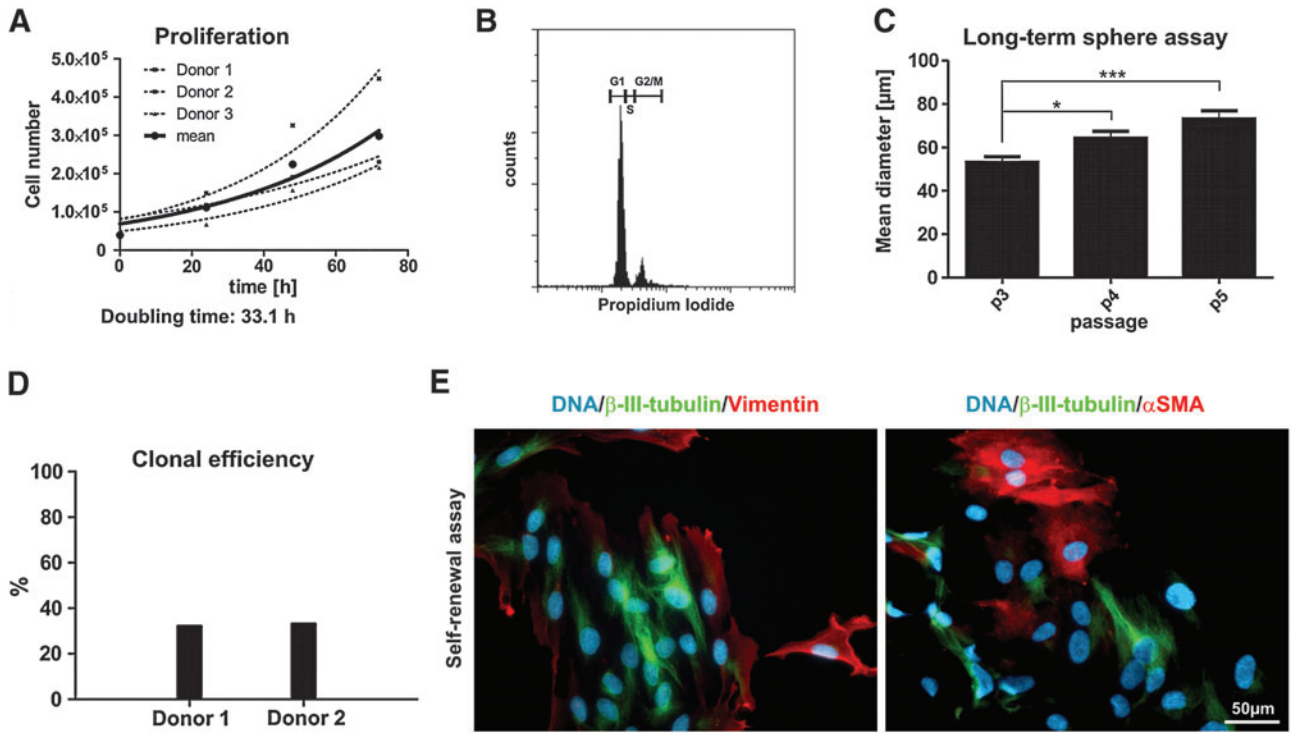

FIG. 5. Characterization of cultivated ITSCs. **(A)** Proliferation of 3 ITSC cultures in defined cultivation medium with 10% blood plasma showed a population doubling time of 33h without morphological signs of differentiation. **(B)** CyFlow analysis of cultivated ITSCs after 90 days of cultivation displayed a typical propidium iodide pattern for diploid cell cultures. **(C)** Long-term sphere formation was analyzed for 3 passages demonstrating an increased diameter of spheres from 53 to 73 µm. **(D)** The ability to renew themselves was investigated by a limited dilution assay of single cells, where ITSCs showed a clonal efficiency of 32.5%. **(E)** Multi-lineage differentiation of tertiary single-cell clones revealed that a single cell clone could differentiate into cells of mesodermal and ectodermal origin visualized by the expression of β-III-tubulin, vimentin and αSMA. Nuclei were stained with TOTO. Scale bar: 50µm.

of ITSCs cultures was analyzed by 2n DNA content for up to 150 days (data not shown).

ITSCs show high clonal efficiency and self-renewal capability

To identify long-term sphere formation the amount and diameter of spheres cultivated over 3 passages was investigated (Fig. 5C) demonstrating an increase of the mean diameter of the spheres from 53 to 73 μm.

Stem cells are characterized by the ability to self-renew. A test for this capability is the analysis of single cell proliferation. Therefore, proliferation of single ITSCs was analyzed with the help of a limited dilution assay via microscopy. Here, ITSCs showed a clonal efficiency of 32.5%, indicating self-renewal capability of these cells (Fig. 5D). To further verify the self-renewal potential of ITSCs, multi-lineage differentiation of tertiary single-cell clones was investigated after addition of 10% FCS (Fig. 5E). Here we were able to show that a clone derived from a single cell could differentiate into cells of mesodermal and ectodermal origin. We could identify clones with no co-expression of β-III-tubulin/vimentin and β-III-tubulin/αSMA. Taken together these data suggest that ITSCs have the capability to self-renew.

ITSCs perform differentiation into ectodermal lineage

To investigate the ectodermal differentiation potential of ITSCs, ITSCs were cultivated in neuronal differentiation medium for 4 weeks (Fig. 6A). Afterward the differentiated ITSCs were analyzed via immunocytochemical stainings, RT-PCR and synaptic vesicle recycling assay. In Fig. 6B the co-expression of neuronal markers β-III-tubulin and Neurofilament-H is clearly detectable using immunocytochemical staining. This staining showed typical neuronal morphology of differentiated ITSCs building up a neuronal

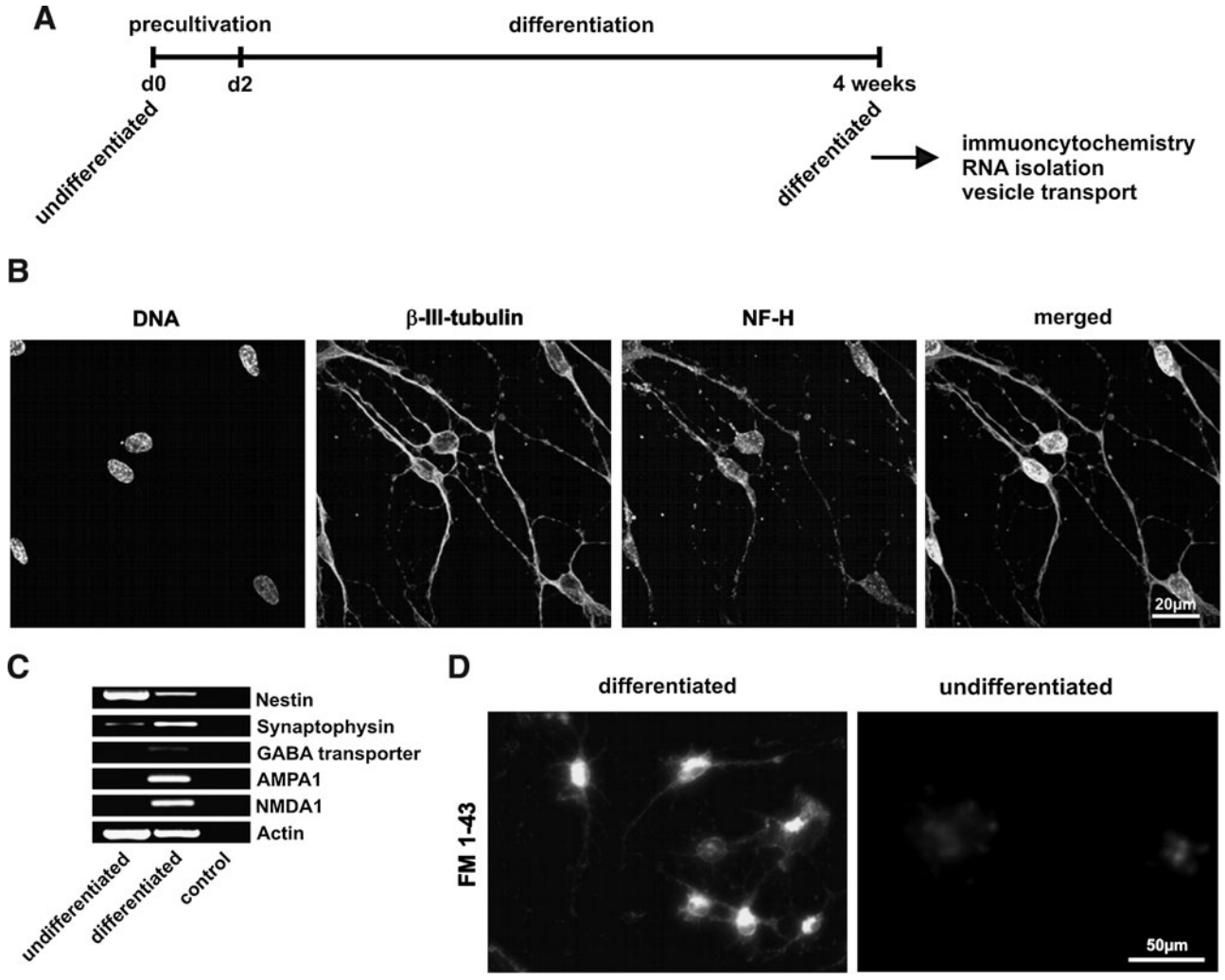

FIG. 6. ITSCs are able to differentiate into neuro-ectodermal lineage **(A)** ITSCs were cultivated in neuronal differentiation medium for 4 weeks to induce neuronal differentiation. **(B)** Neuronally differentiated ITSCs showed typical neuronal morphology and co-expressed neuronal markers β-III-tubulin and Neurofilament-H. Nuclei were stained with TOTO. Scale bar: 20μm. **(C)** RT-PCR showed the downregulation of nestin and upregulation of synaptophysin, and the channels NMDA1, AMPA1, and the GABA transporter. **(D)** The functionality of differentiated neurons was proven by a synaptic vesicle recycling assay resulting in strong labeling with FM1-43 dye in several neurons, while no labeling was detectable in undifferentiated ITSCs. Scale bar: 50μm.

network-like connections. To identify the type of neurons which were differentiated from ITSCs, RT-PCR analysis was performed (Fig. 6C). The downregulation of nestin and upregulation of synaptophysin is a strong evidence for neuronal differentiation. To identify the type of neurons, PCRs for different channels and transporters were performed. A strong expression of AMPA1 and NMDA1 indicates the predominant differentiation of ITSCs into glutamatergic neurons, while the expression of GABA transporter was very low. The functionality of differentiated neurons was investigated by performing synaptic vesicle recycling. Neurons were stimulated and loaded with FM1-43 dye. Active neurons recycle vesicles and by vesicle uptake these neurons were labeled green, while no labeling above the background signal was detectable in undifferentiated ITSCs (Fig. 6D).

ITSCs are able to differentiate into representative mesodermal cell types

To investigate the mesodermal differentiation potential, ITSCs were analyzed after spontaneous multi-lineage differentiation assay. After at least 7 days of cultivation under differentiation-inducing conditions the cells were fixed and processed for immunocytochemistry. The mesodermal cell marker αSMA was detectable in 0.01%±0.005 of the differentiated cells (Fig. 7A).

In addition, several directed mesodermal differentiation protocols were tested to examine whether ITSCs can be efficiently differentiated into mesodermal direction. Adipogenic differentiation could be identified via Oil Red O staining (Fig. 7B). Acidic sulfated mucosubstances (blue) which are a specific for cartilage could be detected with Alcian Blue staining (Fig. 7C). After osteogenic differentiation, strong ALP activity was detectable in differentiated cells (Fig. 7D), but not in controls (data not shown). To investigate mineralization of differentiated ITSCs Von Kossa and Alizarin Red S stainings were performed. Both stainings showed strong signals, while Alizarin Red S confirmed the $Ca2^{+}$-depositions within the differentiated cells.

ITSCs are able to survive and perform neural crest specific chain migration

GFP- or LacZ- transduced ITSCs were transplanted into chicken embryos (Fig. 8A) followed by 3 days of incubation, fixation, and horizontal sectioning. Via X-Gal staining LacZ-positive cells were easily detectable. Sections containing GFP-positive cells were stained using antibodies against human nuclei (huNu).

As demonstrated by chains of GFP/huNu double-positive cells and chains of lacZ positive cells dorsolaterally oriented between the somite and the ectoderm, ITSCs migrate preferably dorsolaterally and not ventrally (Fig. 8B/C). These chains could be identified in 5 of 5 analyzed chick embryos. Chain migration is a typical hallmark of neural crest cells in developmental context [33]. LacZ-HEK293T control cells were not able to migrate and were only diffusely distributed near to the injection site (Fig. 8D).

In addition ITSCs were injected into SCID mice to analyze for potential teratoma formation. In contrast to human

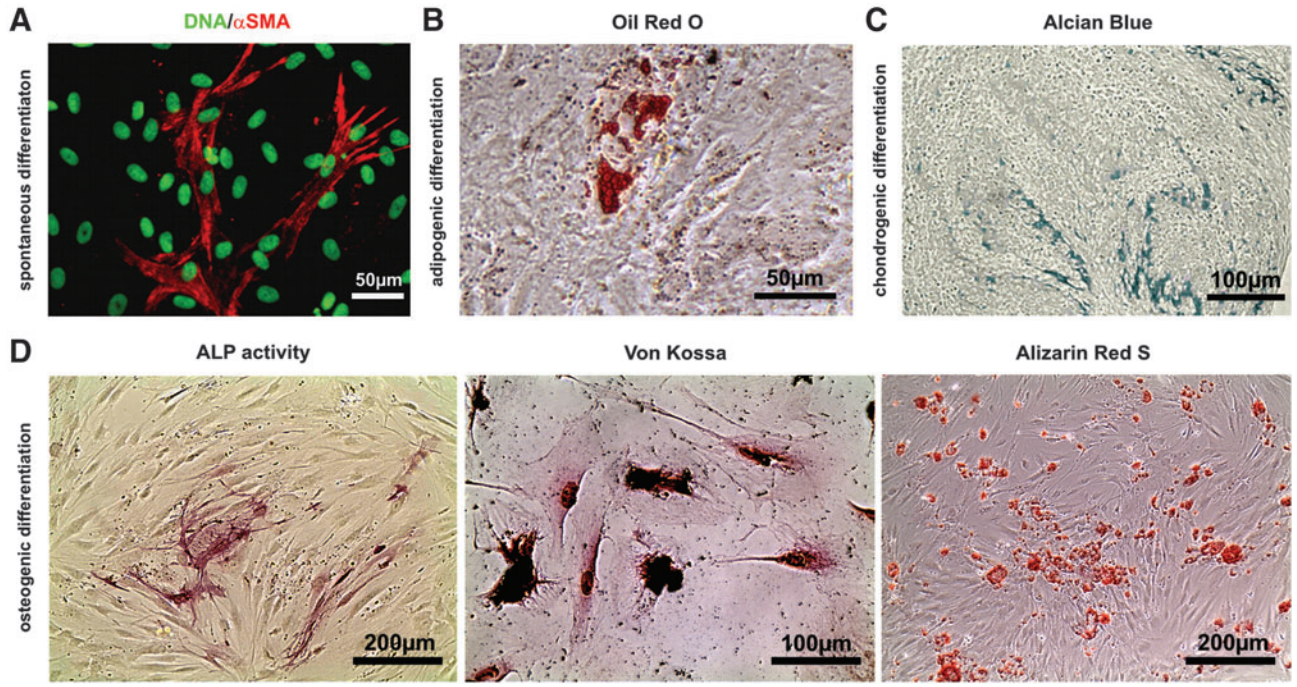

FIG. 7. ITSCs differentiate into several cell types with mesodermal origin **(A)** Spontaneous differentiation revealed that ITSCs could be differentiated into mesodermal lineage demonstrated by αSMA-positive differentiated cells. **(B)** ITSCs can differentiate into adipogenic cell as demonstrated by Oil Red O staining. Scale bar: 50µm. **(C)** ITSCs, cultured as high density pellets showed acidic sulfated mucosubstances (*blue*) visualized Alcian blue staining after chondrogenic differentiation. Scale bar: 100 µm. **(D)** ITSCs, differentiated into osteogenic lineage showed high ALP activity and Osteogenic mineralization visualized by Von Kossa and Alizarin red S stainings. Scale bar: 200µm

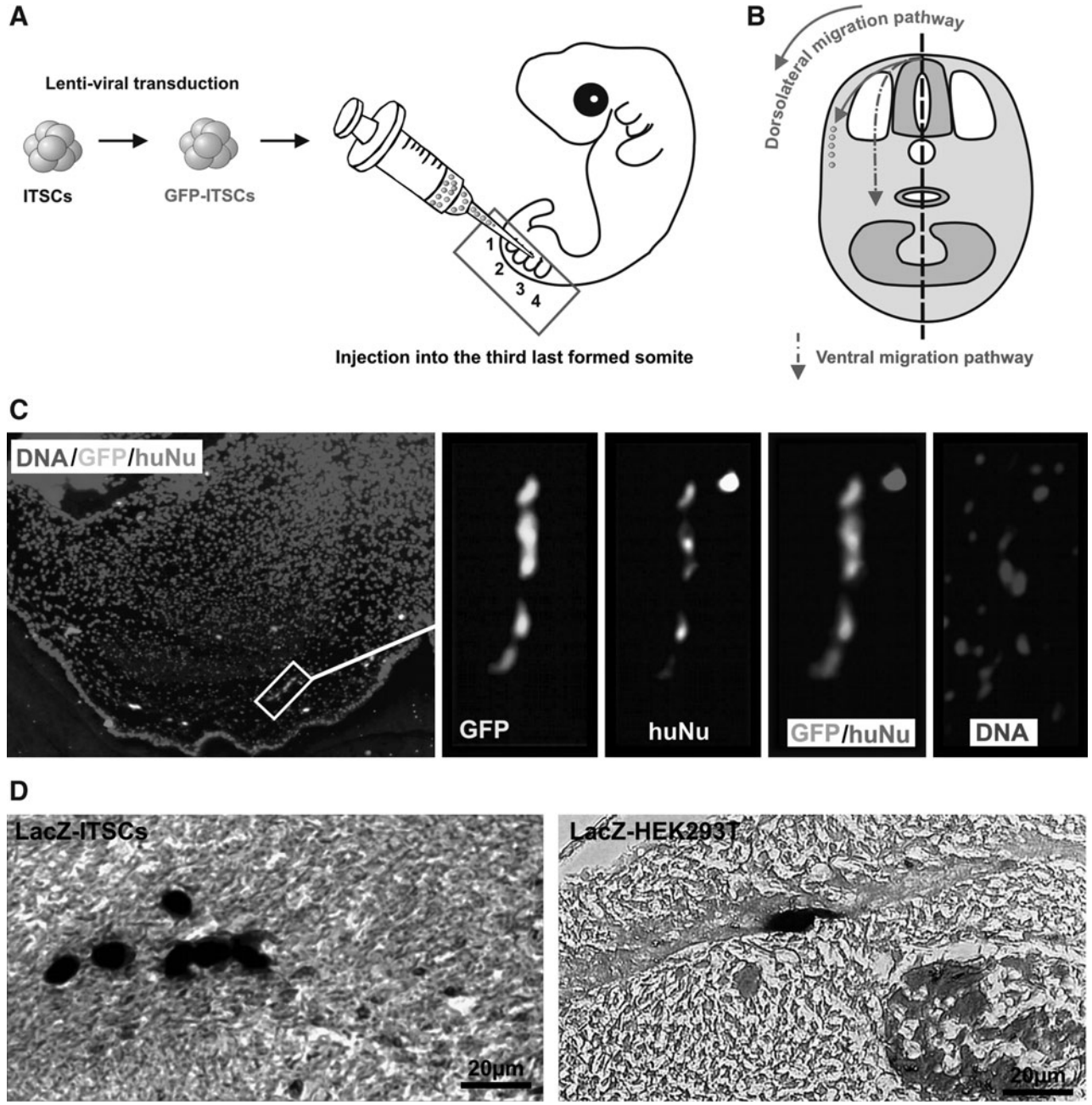

FIG. 8. ITSCs migrate and perform NCSC-typical chain migration **(A)** Schematic illustration of the injection site of the GFP/LacZ transduced ITSCs or HEK293 controls into the third somite of a stage 18 chicken embryo. **(B)** Migration pathways of neural crest cells within developing chicken embryo. Neural crest cells can migrate dorsolaterally or ventrally through the rostral half of each somite. **(C)** GFP-transduced ITSCs survived and performed chain migration after cross-species transplantation in a stage 18 chicken embryo. After 3 days of incubation dorsolateral chain migration became evident as demonstrated by chains of GFP/huNu positive cells. **(D)** LacZ-HEK293T cells were only diffusely distributed near to the injection site, whereas LacZ-ITSCs migrated as chains. Scale bar: 20µm

embryonic stem cell line (hESC-line) and hiPSCs, that give rise to teratoma formation within 6 to 8 weeks [34], no teratoma formation could be detected with the ITSCs.

ITSCs can be efficiently enriched by MACS based on the expression of p75^{NTR}

To establish a purification strategy of adult ITSCs, dissociated tissue samples were analyzed by flow cytometry for the presence of p75^{NTR+} (CD271+) ITSCs. An average percentage of 16.6%±5.1 p75^{NTR}-expressing cells were determined in donors of both genders and of an age of 15–74 years (see Table 1).

Thereafter, magnetic cell sorting (MACS) using p75^{NTR} microbeads was performed with subsequent flow cytometric analysis. Eleven separations were successful, resulting in an average purity of 62.4%±12.4 p75^{NTR+} cells. A flow cytometric analysis of a typical experiment is shown in Fig. 9A.

Table 1. Percentage of p75 Positive Cells Within Freshly Dissociated Tissue. An Average Percentage of 16.5% ± 5.1 Inferior Turbinate Cells Were Positive for $p75^{NTR}$

Donor	*Age*	*Gender*	*Percentage of $p75^{NTR}$-expressing cells*
Donor I	64	M	13.33%
Donor II	62	M	15.32%
Donor III	74	M	12.38%
Donor IV	47	F	20.37%
Donor V	39	M	20.50%
Donor VI	63	F	22.80%
Donor VII	28	M	23.51%
Donor VIII	36	M	16.18%
Donor IX	26	M	16.11%
Donor X	15	M	12.14%
Donor XI	56	M	16.12%
Donor XII	59	M	12.36%
Donor XIII	57	M	10.84%
Donor XIV	41	M	9.78%
Donor XV	30	M	26.50%
Average			16.55 + 5.1%

After separation the isolated negative and positive fractions were cultivated and further analyzed.

$p75^{NTR}$ expressing ITSCs form larger neurospheres and proliferate faster than the negative fractions

$p75^{NTR}$ positive and negative fractions were cultivated as neurospheres under serum-free conditions. After 14 days of cultivation, the positive fractions formed obviously larger neurospheres than the negative fractions (Fig. 9B). Moreover, $p75^{NTR+}$ ITSCs showed significantly shorter population doubling time (34.2h to 58.8h (Fig. 9C)).

Expression pattern of p75NTR positive ITSCs

$p75^{NTR+}$ ITSCs showed similar expression of nestin compared with the negative fraction at RNA and protein level as demonstrated by PCR and immunocytochemistry (Fig. 9D and Supplementary Fig. S6). Moreover, SOX2, KLF4, c-MYC, and NANOG were identically expressed by both fractions. Interestingly, OCT4A was only expressed by $p75^{NTR+}$ ITSCs as demonstrated by PCR (Fig. 9D).

Taken together there were only minor differences in gene expression (~400 genes up- or downregulated) between $p75^{NTR+}$ and $p75^{NTR-}$ ITSCs, as measured by microarray analysis (Supplementary Fig. S7).

Discussion

In this study we show that the human respiratory mucosa of the inferior turbinate contains a novel neural crest-derived stem cell population. Such ITSCs from the human respiratory mucosa could successfully be isolated and cultivated in animal serum-free media. These isolated cells were able to proliferate and generate primary and secondary neurospheres in suitable cultivation media. Primary and secondary neurospheres contained cells which differentiate into cells of neuro-ectodermal and mesodermal phenotype and could be efficiently directed into neuron-like cells. Additionally ITSCs were able to survive and to perform neural crest specific chain migration in vivo when transplanted to chick embryos. Microarray experiments demonstrated comparable expression of WDR5, KLF4, and c-MYC compared with human ES cells, whereas, SOX2, LIN28, and NANOG were decreased. It was possible to isolate an enriched ITSC-population by using the surface marker $p75^{NTR}$ as a target for a MACS.

NCSCs in the head region can be found in a number of adult organs and tissues. This is largely because during human embryonic development the cranial part is mainly shaped by migrating neural crest cells [35]. In the last couple of years several NCSC-populations within the cranial part were described. Such cells were identified within hair follicles of the dermal papilla of adult skin [11] and cultivated in medium containing 10% FCS. However, for a potential clinical use, cultivation without FCS is essential. Recently, NCSCs were identified within dental pulp and the periodontal ligament [14,15]. Due to the limited source material these stem cells are not ideal candidates for clinical use. A promising source of NCSCs was detected within the hard palate of adult rat [15]. This study identified nestin/Sox2 positive NCSCs within the adult palatal mucosa. In the hard and soft palate of humans similar NCSCs could be identified [15], which generated neurospheres and were positive for nestin. However, human pNCSCs were not able to generate secondary neurospheres and human palatal tissues were frequently contaminated with bacteria or yeast (unpublished data).

A well studied adult stem cell type within the nasal cavity are the OECs [36–38]. Genetic tracing demonstrated that OECs are directly formed by neural crest cells and therefore are neural crest-derived [17]. A further population of adult stem cells within the olfactory mucosa was recently discovered [39]. The so called olfactory mucosa mesenchymal stem cells (OE-MSCs) expressed high levels of nestin, CD54, and CD90. In addition, OE-MSCs were negative for the IL-6 receptor CD126. OE-MSCs could successfully be differentiated in osteo- and adipogenic direction, while no chondrogenic differentiation was observed. In contrast to OE-MSCs, ITSCs are negative for CD54 (data not shown), express CD126 (see microarrays), and could be efficiently differentiated into chondrogenic cells, suggesting that OE-MSCs and ITSCs are different cell types with similar, but not identical developmental potential. Although OECs and OE-MSCs are very plastic, they are located in humans within the lamina propria of olfactory epithelium, which covers a total area of only about 3% of the total surface area of the nasal cavity in humans, and are wrapped in bundles around axons [40]. Human adult olfactory epithelium is gradually replaced by respiratory epithelium during aging [25]. Therefore a random biopsy of the olfactory region does not assure a pure source of olfactory epithelium [41,42]. In contrast to the olfactory bulb and the superior/middle turbinates, the human inferior turbinate exclusively contains respiratory epithelium lacking OECs and OE-MSCs. However, [43] recently demonstrated that transplanted grafts of human inferior turbinates are able to close nasal septal perforations (Mansour) indicating a presence of stem cells within the respiratory mucosa.

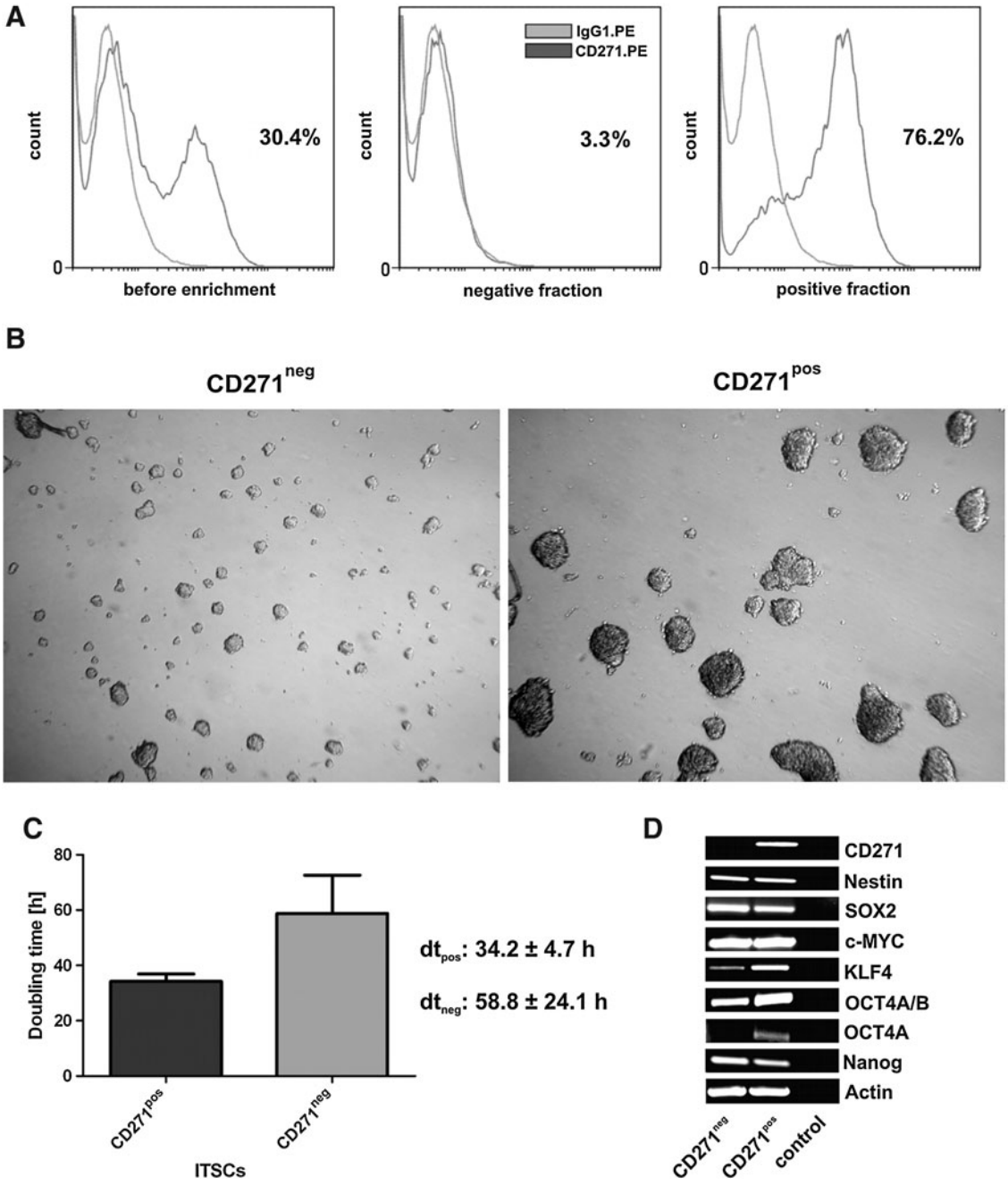

FIG. 9. ITSCs can be efficiently enriched by magnetic cell sorting (MACS) based on the expression of $p75^{NTR}$. **(A)** Before enrichment 30.4% $p75^{NTR}$ expressing cells were determined. After MACS only 3.3% cells in the negative fraction and the majority of 76.2% cells in the positive fraction showed the expression of $p75^{NTR}$. **(B, C)** $p75^{NTR+}$ sorted ITSCs formed larger neurospheres and proliferate faster than the negative fractions. **(D)** Reverse transcriptase PCR analysis showed the expression of the stemness marker nestin and the "pluripotency factors" in both fractions, whereas Oct4A and p75 are only present in $p75^{NTR+}$ cells. cDNA was normalized using the housekeeping gene β-Actin.

Here we described a novel NCSC-population within adult human inferior turbinate. In contrast to OECs, ITSCs from the respiratory mucosa can be detected even in elderly patients. Stem cells from the inferior turbinate could be isolated age-independent from individuals aged 4–76 years. Such ITSCs represent a novel nonepithelial, cytokeratin negative stem cell population distinct from OECs. OECs have been described to express αSMA in vitro and in vivo [32]. ITSCs were negative for αSMA before and after cultivation. Additionally the neural crest origin of ITSCs could be proven by several neural crest specific markers.

Via the analysis of SOX10, Slug, and p75 expression we provided strong evidences for a neural crest origin of ITSCs.

Further most ITSC cultures showed a robust and high expression of WDR5, KLF4, and c-MYC whereas OCT4 and SOX2 are expressed at lower level compared with hESCs. These transcription factors are sufficient for cellular reprogramming of murine and human skin fibroblast into a

pluripotent state [44–47]. The expression of these transcription factors seems not to be limited to embryonic stem cells and induced pluripotent stem cells, since a weak expression of these pluripotency factors has been reported in NCSCs like epidermal NCSCs and palatal NCSCs [48,16]. Interestingly, EPI-NCSCs express OCT4 at 524-fold lower level compared with ESCs. This is in accordance with our data, since ITSC express OCT4 at 801-fold lower level compared with hESCs. In addition Sieber-Blum showed that EPI-NCSCs grafted into the adult spinal cord do not form tumors [49]. Similarly, ITSCs injected into SCID mice were not able to create teratomas. This might be due to lower expression of OCT4 and SOX2 compared with pluripotent human embryonic stem cells.

Limited dilution assay showed a secondary sphere forming frequency of 32.5%. Interestingly the clonal efficiency of rat pNCSCs is only about 1.8% [16]. In contrast, highly enriched rodent skin-precursors (SKPs) isolated from dermal papilla formed secondary neurospheres with a frequency of 24.4% [11]. This suggests that ITSCs harbor a clonal efficiency comparable to SKPs and appear to be more potent than pNCSCs. However, such fast cycling ITSCs showed no aberrant DNA content even after 150 days of cultivation. To validate the differentiation potential of ITSCs, spontaneous and directed differentiation assays were utilized. If cultivated in presence of 10% FCS, a moderate number of cells were able to differentiate into the mesodermal cell lineage. Directed neuronal and mesodermal differentiation assays revealed an efficient differentiation into neuronal, adipogenic, chondrogenic, and osteogenic cell types. For therapeutic applications an efficient generation of a specific cell type might be important for the success of a therapy. Injection of ITSCs into chicken embryos leads to dorsolaterally orientated chain migration between the somite and the ectoderm. This is a specific hallmark for neural-crest related stem cells; in contrast neural stem cells migrate as single cells [33].

Concerning the potential clinical use of stem cells, a pure, precisely defined, and enriched population is needed. Since $p75^{NTR}$ is a cell surface receptor and expressed by ITSCs in vivo, it is a promising candidate for a sorting strategy. We decided to separate ITSCs using MACS method with post-hoc verification of the purity by flow cytometry. In freshly dissociated tissue, an average percentage of $16.5\% \pm 5.1$ inferior turbinate cells were positive for $p75^{NTR}$ (Table 1), independent of donor age and gender. After separation, up to 76.2% of the cells within the positive sorted fraction could be identified as $p75^{NTR+}$ (Fig. 9A). When cultivated; both—the negative and positive fractions—were positive for nestin, whereas only the positive fraction expressed p75 and OCT4A. It could be demonstrated in the central nervous system that $p75^{NTR+}$ neural stem cells (NSC) form larger neurospheres and proliferate much faster compared with the $p75^{NTR-}$ NSC population [50]. Our results suggest that the $p75^{NTR+}$ stem cell population forms larger neurospheres and shows reduced population doubling time.

Taken together our study indicates that the novel identified ITSCs are an unique and promising, easily accessible neural crest-related stem cell source, which can be isolated and cultivated in a sufficient amount with a high yield and purity and therefore are future candidates for the therapy of craniofacial lesions.

Acknowledgments

The excellent technical help of Angela Krahlemann-Köhler is gratefully acknowledged. We thank PARTEC GmbH for support and Dr. K. Rott (Department of Physics, University of Bielefeld) for his help with scanning electron microscopy. This study was supported by a grant of the German Ministry of Research and Education (BMBF, grant: 01GN1006A, to Barbara Kaltschmidt).

Author Disclosure Statement

No competing financial interests exists.

References

1. His W. (1868). Untersuchungen über die erste Anlage des Wirbeltierleibes. Die erste Entwicklung des Hühnchens im Ei. Leipzig, Vogel.
2. Le Douarin NM, GW Calloni and E Dupin. (2008). The stem cells of the neural crest. Cell Cycle 7:1013–1019.
3. Shakhova O and L Sommer. (2010). Neural crest-derived stem cells. In: *StemBook*. Gage FH and FM Watt, eds. Harvard Stem Cell Institute, Cambridge. DOI: doi/10.3824/stembook.1.51.1.
4. Trentin A, C Glavieux-Pardanaud, NM Le Douarin, et al. (2004). Self-renewal capacity is a widespread property of various types of neural crest precursor cells. Proc Natl Acad Sci U S A 101:4495–4500.
5. Sieber-Blum M and AM Cohen. (1980). Clonal analysis of quail neural crest cells: they are pluripotent and differentiate in vitro in the absence of noncrest cells. Dev Biol 80:96–106.
6. Stemple DL and DJ Anderson. (1992). Isolation of a stem cell for neurons and glia from the mammalian neural crest. Cell 71:973–985.
7. Bronner-Fraser M, M Sieber-Blum and AM Cohen. (1980). Clonal analysis of the avian neural crest: migration and maturation of mixed neural crest clones injected into host chicken embryos. J Comp Neurol 193:423–434.
8. Le Douarin NM and MA Teillet. (1974). Experimental analysis of the migration and differentiation of neuroblasts of the autonomic nervous system and of neurectodermal mesenchymal derivatives, using a biological cell marking technique. Dev Biol 41:162–184.
9. Dupin E, GW Calloni and NM Le Douarin. (2011). The cephalic neural crest of amniote vertebrates is composed of a large majority of precursors endowed with neural, melanocytic, chondrogenic and osteogenic potentialities. Cell Cycle 9:238–249.
10. Brandl C, C Florian, O Driemel, et al. (2009). Identification of neural crest-derived stem cell-like cells from the corneal limbus of juvenile mice. Exp Eye Res 89:209–217.
11. Hunt DP, PN Morris, J Sterling, et al. (2008). A highly enriched niche of precursor cells with neuronal and glial potential within the hair follicle dermal papilla of adult skin. Stem Cells 26:163–172.
12. Techawattanawisal W, K Nakahama, M Komaki, et al. (2007). Isolation of multipotent stem cells from adult rat periodontal ligament by neurosphere-forming culture system. Biochem Biophys Res Commun 357:917–923.
13. Toma JG, M Akhavan, KJ Fernandes, et al. (2001). Isolation of multipotent adult stem cells from the dermis of mammalian skin. Nat Cell Biol 3:778–784.
14. Waddington RJ, SJ Youde, CP Lee, et al. (2009). Isolation of distinct progenitor stem cell populations from dental pulp. Cells Tissues Organs 189:268–274.

15. Widera D, WD Grimm, JM Moebius, et al. (2007). Highly efficient neural differentiation of human somatic stem cells, isolated by minimally invasive periodontal surgery. Stem Cells Dev 16:447–460.
16. Widera D, C Zander, M Heidbreder, et al. (2009). Adult palatum as a novel source of neural crest-related stem cells. Stem Cells 27:1899–1910.
17. Barraud P, AA Seferiadis, LD Tyson, et al. (2011). Neural crest origin of olfactory ensheathing glia. Proc Natl Acad Sci U S A 107:21040–21045.
18. Tome M, SL Lindsay, JS Riddell, et al. (2009). Identification of nonepithelial multipotent cells in the embryonic olfactory mucosa. Stem Cells 27:2196–2208.
19. Murrell W, F Feron, A Wetzig, et al. (2005). Multipotent stem cells from adult olfactory mucosa. Dev Dyn 233:496–515.
20. Mackay-Sim A. (2011). Stem cells and their niche in the adult olfactory mucosa. Arch Ital Biol 148:47–58.
21. Nakane PK, and A Kawaoi. (1974). Peroxidase-labeled antibody. A new method of conjugation. J Histochem Cytochem 22:1084–1091.
22. Danscher G. (1981). Localization of gold in biological tissue. A photochemical method for light and electronmicroscopy. Histochemistry 71:81–88.
23. Irizarry RA, BM Bolstad, F Collin, et al. (2003). Summaries of Affymetrix GeneChip probe level data. Nucleic Acids Res 31:e15.
24. Edgar R, M Domrachev and AE Lash. (2002). Gene expression omnibus: NCBI gene expression and hybridization array data repository. Nucleic Acids Res 30:207–210.
25. Linta L, M Stockmann, KN Kleinhans, et al. (2011). Rat embryonic fibroblasts improve reprogramming of human keratinocytes into induced pluripotent stem cells. Stem Cells Dev [Epub ahead of print]; doi:10.1089/scd.2011.0026.
26. Nakashima T, CP Kimmelman and JB Snow, Jr. (1984). Structure of human fetal and adult olfactory neuroepithelium. Arch Otolaryngol 110:641–646.
27. Bruch RC and VM Carr. (1991). Rat olfactory neurons express a 200 kDa neurofilament. Brain Res 550:133–136.
28. Lee VM and SK Pixley. (1994). Age and differentiation-related differences in neuron-specific tubulin immunostaining of olfactory sensory neurons. Brain Res Dev Brain Res 83:209–215.
29. Minovi A, M Witt, A Prescher, et al. (2010). Expression and distribution of the intermediate filament protein nestin and other stem cell related molecules in the human olfactory epithelium. Histol Histopathol 25:177–187.
30. Witt M, K Bormann, V Gudziol, et al. (2009). Biopsies of olfactory epithelium in patients with Parkinson's disease. Mov Disord 24:906–914.
31. Barber PC and D Dahl. (1987). Glial fibrillary acidic protein (GFAP)-like immunoreactivity in normal and transected rat olfactory nerve. Exp Brain Res 65:681–685.
32. Jahed A, JW Rowland, T McDonald, et al. (2007). Olfactory ensheathing cells express smooth muscle alpha-actin *in vitro* and *in vivo*. J Comp Neurol 503:209–223.
33. Durbec P and G Rougon. (2001). Transplantation of mammalian olfactory progenitors into chick hosts reveals migration and differentiation potentials dependent on cell commitment. Mol Cell Neurosci 17:561–576.
34. Kim JB, V Sebastiano, G Wu, et al. (2009b). Oct4-induced pluripotency in adult neural stem cells. Cell 136:411–419.
35. Santagati F and FM Rijli. (2003). Cranial neural crest and the building of the vertebrate head. Nat Rev Neurosci 4:806–818.
36. Franssen EH, FM de Bree and J Verhaagen. (2007). Olfactory ensheathing glia: their contribution to primary olfactory nervous system regeneration and their regenerative potential following transplantation into the injured spinal cord. Brain Res Rev 56:236–258.
37. Kocsis JD, KL Lankford, M Sasaki, et al. (2009). Unique *in vivo* properties of olfactory ensheathing cells that may contribute to neural repair and protection following spinal cord injury. Neurosci Lett 456:137–142.
38. Lindsay SL, JS Riddell and SC Barnett. (2010). Olfactory mucosa for transplant-mediated repair: a complex tissue for a complex injury? Glia 58:125–134.
39. Delorme B, E Nivet, J Gaillard, et al. (2010). The human nose harbors a niche of olfactory ectomesenchymal stem cells displaying neurogenic and osteogenic properties. Stem Cells Dev 19:853–866.
40. Sorokin S. (1988). The respiratory system. In: *A textbook of histology*. Weiss L, ed. Baltimore, Urban & Schwarzenberg, pp. 751–814.
41. Feron F, C Perry, JJ McGrath, et al. (1998). New techniques for biopsy and culture of human olfactory epithelial neurons. Arch Otolaryngol Head Neck Surg 124:861–866.
42. Paik SI, MN Lehman, AM Seiden, et al. (1992). Human olfactory biopsy. The influence of age and receptor distribution. Arch Otolaryngol Head Neck Surg 118:731–738.
43. Mansour HA. (2011). Repair of nasal septal perforation using inferior turbinate graft. J Laryngol Otol 125:1–5.
44. Ang YS, SY Tsai, DF Lee, et al. (2011). Wdr5 mediates self-renewal and reprogramming via the embryonic stem cell core transcriptional network. Cell 145:183–197.
45. Kim JB, B Greber, Arauzo-Bravo, M.J., et al. (2009a). Direct reprogramming of human neural stem cells by OCT4. Nature 461:649–643.
46. Takahashi K, K Tanabe, M Ohnuki, et al. (2007). Induction of pluripotent stem cells from adult human fibroblasts by defined factors. Cell 131:861–872.
47. Takahashi K and S Yamanaka. (2006). Induction of pluripotent stem cells from mouse embryonic and adult fibroblast cultures by defined factors. Cell 126:663–676.
48. Sieber-Blum M and Y Hu. (2008). Epidermal neural crest stem cells (EPI-NCSC) and pluripotency. Stem Cell Rev 4:256–260.
49. Sieber-Blum M, L Schnell, M Grim, et al. (2006). Characterization of epidermal neural crest stem cell (EPI-NCSC) grafts in the lesioned spinal cord. Mol Cell Neurosci 32:67–81.
50. Young KM, TD Merson, A Sotthibundhu, et al. (2007). p75 neurotrophin receptor expression defines a population of BDNF-responsive neurogenic precursor cells. J Neurosci 27:5146–5155.

Address correspondence to:
Dr. Barbara Kaltschmidt
Molecular Neurobiology
University of Bielefeld
Universitätsstr. 25
D-33501 Bielefeld
Germany

E-mail: barbara.kaltschmidt@uni-bielefeld.de

Received for publication August 1, 2011
Accepted after revision November 30, 2011
Prepublished on Liebert Instant Online November 30, 2011